Anisotropic electrical and magnetic properties of CeTSb$_2$ (T=Cu, Au, and Ni) single crystals

Arumugam Thamizhavel,[1] Tetsuya Takeuchi,[2] Tomoyuki Okubo,[1] Mineko Yamada,[1] Rihito Asai,[1] Shingo Kirita,[1] Andrei Galatanu,[3] Etsuji Yamamoto,[3] Takao Ebihara,[4] Yoshihiko Inada,[1] Rikio Settai,[1] and Yoshichika Onuki[1,3]

[1]*Graduate School of Science, Osaka University, Toyonaka, Osaka 560-0043, Japan*

[2]*Low Temperature Center, Osaka University, Toyonaka, Osaka 560-0043, Japan*

[3]*Advances Science Research Center, Japan Atomic Energy Research Institute, Tokai, Ibaraki 319-1195, Japan*

[4]*Department of Physics, Faculty of Science, Shizuoka University, 836 Ohya, Shizuoka 422-8529, Japan*

(Received 5 November 2002; revised manuscript received 11 March 2003; published 26 August 2003)

In order to understand the anisotropic magnetic and electrical properties of ternary compounds CeTSb$_2$ (T=Cu, Au, Ni) with the tetragonal structure, we have grown single crystals of this series by the self-flux method and measured the electrical resistivity, magnetic susceptibility, magnetization, and specific heat. CeCuSb$_2$ and CeAuSb$_2$ are found to order antiferromagnetically with Néel temperatures of 6.9 K and 5.0 K, respectively, while CeNiSb$_2$ is a ferromagnet with a Curie temperature of 6.0 K with an easy axis of magnetization oriented along the [100] direction. The magnetic property of CeCuSb$_2$ shows a very small anisotropy, whereas the electrical resistivity is highly anisotropic between $J\|$ [100] and [001]. In contrast, CeAuSb$_2$ and CeNiSb$_2$ show a strong anisotropy both in the magnetic and electrical measurements, although the magnetic easy axis is interchanged with respect to each other. The anisotropy in the magnetic properties has been explained on the basis of a crystalline electric-field model.

DOI: 10.1103/PhysRevB.68.054427 PACS number(s): 71.20.Eh, 71.27.+a, 71.70.Ch, 75.50.Gg

I. INTRODUCTION

Recently rare-earth and uranium compounds with a quasi-two-dimensional electronic state have been attracting wide attention in relation to superconductivity.[1–3] CeCoIn$_5$ and CeIrIn$_5$ are heavy-fermion superconductors with transition temperatures of 2.3 K and 0.4 K, respectively. It is noted that CeCoIn$_5$ is the first *f*-electron superconductor of which the position of nodes in the superconducting energy gap was determined, indicating a $d_{x^2-y^2}$ type.[4] There are other compounds with quasi-two-dimensionality: RX_2 (R—rare earth, X—pnictogen), UX_2, UTGa$_5$ (T—transition metal), and Ce$T X$.[5–7] The quasi-two-dimensional electronic state in UX_2, CeTIn$_5$, and UTGa$_5$ is closely related to the magnetic unit cell and/or the unique crystal structure elongated along the tetragonal [001] direction, which bring about flat Brillouin zones and produce cylindrical but highly corrugated Fermi surfaces along [001].

CeTSb$_2$ or more generally RTX_2 and UTX_2, as discussed by Kaczorowski *et al.*,[8] crystallize in the tetragonal ZrCuSi$_2$-type structure (space group $P4/nmm$), which can be described as a filled UX_2 in UTX_2: planes of transition-metal atoms intercalate into the unit cell of the respective binary uranium dipnictide. The crystal structure of CeTSb$_2$ can also be understood from the stacking arrangement of CeSb-T-CeSb-Sb layers,[9] as shown in Fig. 1. Although there are some reports on the CeTSb$_2$ compounds, most of them are on polycrystalline samples,[10–12] except for CeAgSb$_2$,[13] and their magnetic properties are not clearly elucidated.

Recently, we have carried out the de Haas–van Alphen (dHvA) experiment, together with the electrical resistivity, magnetic susceptibility, magnetization, and specific-heat experiments on a high-quality single-crystal CeAgSb$_2$ which has a small net ferromagnetic moment of $0.4\mu_B$/Ce.[14] The bulk magnetic properties are well explained by the crystalline electric-field (CEF) scheme.[15] On the other hand, large dHvA frequencies of 10^8 Oe, which correspond to cylindrical Fermi surfaces, were detected by the dHvA measurement for the magnetic field along the tetragonal [001] direction, indicating the quasi-two-dimensional electronic structure. The dHvA branches in CeAgSb$_2$ are highly different from those with small dHvA frequencies of 10^7 Oe in the reference compounds LaAgSb$_2$ and YAgSb$_2$ which exhibit a semimetallic character. The dHvA results have been compared with the results of the energy-band calculations. It was concluded that the $4f$ electron is mainly localized, and the Fermi surface of CeAgSb$_2$ is similar to that of LaAgSb$_2$, except for a slight enlargement which enabled it to form the large orbits along a hollow cylindrical Fermi surface.[14]

In order to understand the physical properties of the other CeTSb$_2$ (T=Cu, Au, and Ni) unambiguously, we have

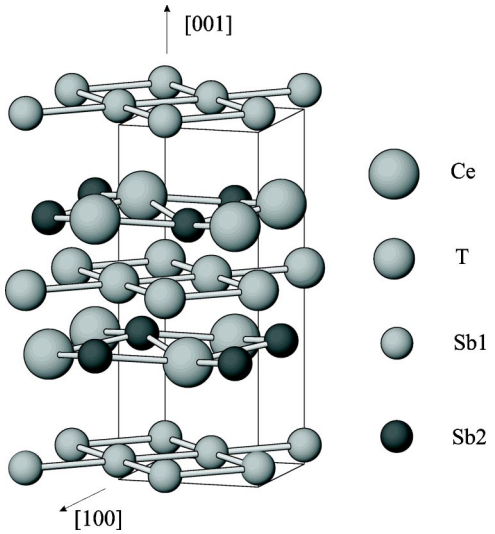

FIG. 1. Crystal structure of CeTSb$_2$ (T=Cu, Au and Ni).

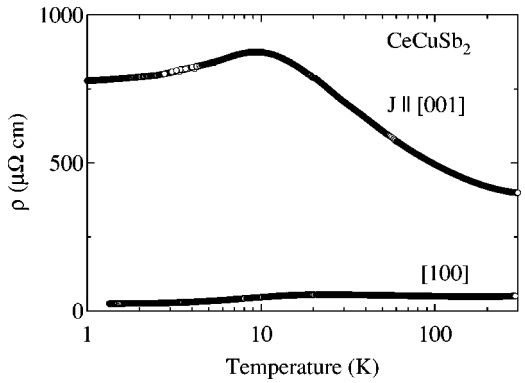

FIG. 2. Temperature dependence of the electrical resistivity of $CeCuSb_2$.

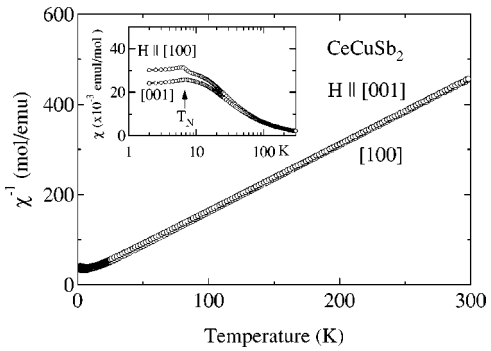

FIG. 3. (a) Temperature dependence of the inverse magnetic susceptibility of $CeCuSb_2$. The inset shows the magnetic susceptibility.

grown single crystals and investigated the magnetic and electrical properties by studying the heat capacity, anisotropic resistivity, and magnetization along the two crystallographic directions. We have also performed the CEF analysis of the magnetic susceptibility and magnetization data on these single crystals to understand the variation in the magnetic properties due to the transition metals.

II. EXPERIMENT

Single crystals were grown by the self-flux method, as described in Ref. 13. The starting materials with 3N (99.9% pure)-Ce, 5N-Cu and Au, 4N-Ni and 5N-Sb were taken in the appropriate ratio with excess Sb as a flux. The starting materials were then placed in an alumina crucible and sealed inside an evacuated quartz ampoule with a partial pressure of Ar. The temperature of the furnace was raised to 1000 °C and after homogenizing the mixture for two days, the furnace was cooled down to the eutectic temperature over a period of three weeks and then rapidly to room temperature. The crystals were separated from the flux by means of a centrifuge. The typical size of the crystal was $8\times5\times3$ mm^3, being flat in the (001) plane. The single-crystalline nature was confirmed by x-ray Laue back reflection technique and the crystals were cut along the desired orientation by means of a spark erosion cutter. As mentioned in the Introduction, these compounds crystallize in the tetragonal structure with lattice constants, $a=4.337$ Å and $c=10.233$ Å for $T=$Cu, $a=4.408$ Å and $c=10.339$ Å for $T=$Au, and $a=4.393$ Å and $c=9.750$ Å for $T=$Ni.[10]

The electrical resistivity was measured by the four-probe dc method, magnetic susceptibility and magnetization were measured by the commercial superconducting quantum interference device magnetometer and the specific heat was measured by the quasiadiabatic heat-pulse method.

III. EXPERIMENTAL RESULTS

A. $CeCuSb_2$

Figure 2 shows the temperature dependence of the electrical resistivity ρ from about 1 K to 300 K. The electrical resistivity is highly anisotropic between $J\|$ [100] and [001], reflecting the quasi-two-dimensional electronic state. The resistivity also shows a $-\ln T$ dependence with decreasing temperature, indicating that this compound forms a dense Kondo lattice. The resistivity has a maximum around 23 K for $J\|$ [100] and around 9 K for $J\|$ [001], and decreases further with decreasing the temperature. The maximum in the resistivity and the subsequent fall may arise due to the onset of coherence among the Ce ions. This is typical of heavy fermion compounds as in the case of $CeCu_6$.[16] The magnetic susceptibility and the heat-capacity studies (described later in this section) show antiferromagnetic ordering below 6.9 K. However, the evidence for the transition is not discernible from the resistivity data.

The temperature dependence of the magnetic susceptibility in a field of 1 T from 2 K to 300 K is shown in the inset of Fig. 3. The susceptibility shows a very small anisotropy along the two crystallographic directions, which is contrary to the resistivity data. However, the antiferromagnetic ordering can be identified by the peak at $T_N=6.9$ K. The high-temperature data exhibit the Curie-Weiss behavior in the paramagnetic region above 100 K, as shown in Fig. 3. The effective magnetic moment $\mu_{\rm eff}$ and the paramagnetic Curie temperature θ_p are estimated to be $2.32\mu_B$/Ce and -12 K, respectively, for $H\|$ [100] and $2.33\mu_B$/Ce and -17 K, respectively, for $H\|$ [001]. The effective magnetic moment is slightly smaller than the free ion moment of Ce^{3+} ($2.54\mu_B$/Ce). The negative sign of the paramagnetic Curie temperatures indicates an antiferromagnetic correlation of this compound. We have also estimated the average of mag-

TABLE I. Magnetic ordering temperature $T_{\rm ord}$, the average of the effective magnetic moment $\mu_{\rm eff}$, the paramagnetic Curie temperature θ_p, and specific-heat coefficient γ of CeTSb$_2$ ($T=$Cu, Ag, Au, and Ni). The data of $CeAgSb_2$ are cited from Ref. 14. (Where AF means antiferromagnetic and F means ferromagnetic.)

		$T_{\rm ord}$ (K)	$\mu_{\rm eff}$ (μ_B/Ce)	θ_p (K)	γ (mJ/K^2 mol)
$CeCuSb_2$	AF	6.9	2.33	−9	100
$CeAgSb_2$	F	9.7	2.47	4.3	46
$CeAuSb_2$	AF	5.0	2.45	−22	90
$CeNiSb_2$	F	6.0	2.33	−22	55

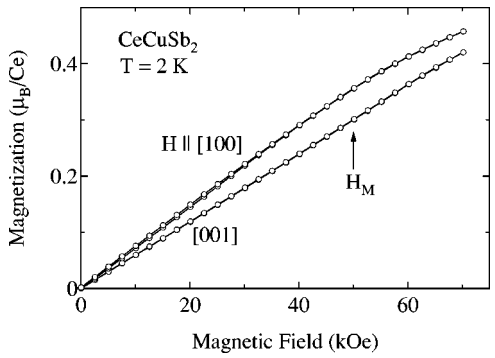

FIG. 4. Field dependence of the magnetization in $CeCuSb_2$.

netic susceptibility using the relation $\chi_{ave}=(2\chi_{[100]}+\chi_{[001]})/3$, and the corresponding effective magnetic moment and the paramagnetic Curie temperature are tabulated in Table I. Below 100 K, the χ^{-1} data of $CeCuSb_2$ is curvillinear, which could be due to the combined influence of CEF and Kondo effect.

Figure 4 shows the magnetization curves at 2 K along two principal directions. A magnetic moment at a field of 70 kOe only amounts to $0.4\mu_B$/Ce–$0.5\mu_B$/Ce, significantly reduced because the magnetic moment of $1.0\mu_B$/Ce is commonly observed in ternary intermetallics. There is slightly a metamagnetic transition for $H\|$ [001] at $H_M=50$ kOe, shown by an arrow, while the magnetization for $H\|$ [100] tends to saturate at high fields. From these data we deduce [001] as the antiferromagnetic easy axis. However, data at much higher fields are necessary to clarify it.

The temperature dependence of the heat capacity in the form of C/T versus T is shown in Fig. 5. The bulk magnetic ordering at $T_N=6.9$ K is unambiguously established from the specific-heat data. The C/T data below about 5 K decrease almost linearly with decreasing temperature. A linear extrapolation to $T=0$ gives a relatively large electronic specific-heat coefficient $\gamma\sim 100$ mJ/K^2 mol, as shown in Fig. 5 by a broken line. The enhanced γ value is due to the Kondo effect. Also shown in Fig. 5 is the total entropy change of $CeCuSb_2$. The entropy change at low temperatures, which is shown by a solid line, is estimated by assuming the linear temperature dependence of C/T, as shown by

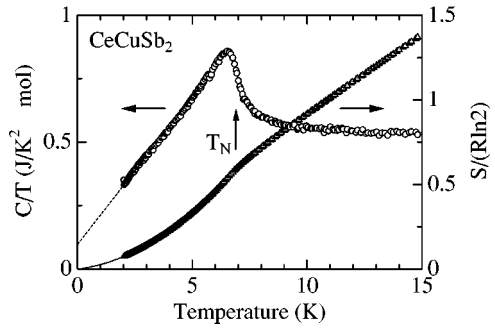

FIG. 5. Temperature dependence of the specific heat in the form of C/T and the total entropy of $CeCuSb_2$. The broken line shows a linear extrapolation of C/T vs T data below 5 K, and the solid line displays the corresponding entropy change below 2 K.

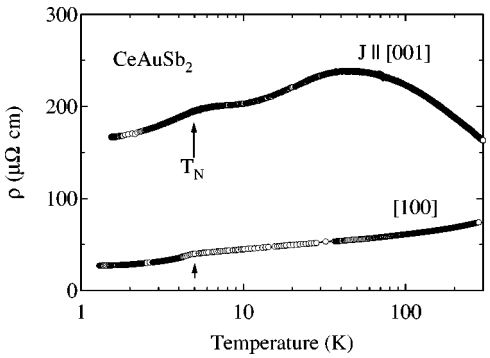

FIG. 6. Temperature dependence of the electrical resistivity in $CeAuSb_2$.

the broken line in Fig. 5. Since we do not have the specific-heat data of the corresponding lattice contribution and due to the lack of any reliable data in the literature for the estimation of lattice contribution, we have calculated the total entropy change. Furthermore, we found from our earlier study on $CeAgSb_2$[14] that there is not much difference between the magnetic entropy ($S_{mag}=0.88R\ln 2$) and the total entropy ($S_{total}=0.91R\ln 2$) at the ordering temperature of 9.7 K, and anticipating a similar trend for $CeTSb_2$ (T=Cu, Au, and Ni), we have calculated the total entropy change. The total entropy change for $CeCuSb_2$ at T_N amounts to only about $0.6R\ln 2$. The reduced value of the entropy may be due to the existence of magnetic fluctuations above T_N and due to the presence of the Kondo effect.

B. $CeAuSb_2$

Figure 6 shows the temperature dependence of electrical resistivity for the current directions parallel to [100] and [001] from 1.3 K to 300 K. The magnetic ordering temperature $T_N=5.0$ K can be seen by a change of slope in the resistivity. This compound also exhibits a large anisotropy and $-\ln T$ dependence with decreasing temperature above 100 K for $J\|$ [001], similar to $CeCuSb_2$.

The temperature dependence of the magnetic susceptibility and the inverse susceptibility are shown in Fig. 7. The susceptibility clearly indicates the antiferromagnetic ordering below $T_N=5.0$ K, showing a steep decrease for $H\|$ [001]. The antiferromagnetic easy axis is thus determined as [001].

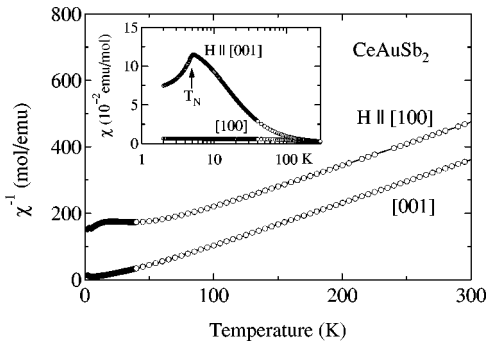

FIG. 7. Inverse magnetic susceptibility of $CeAuSb_2$. The inset shows the magnetic susceptibility.

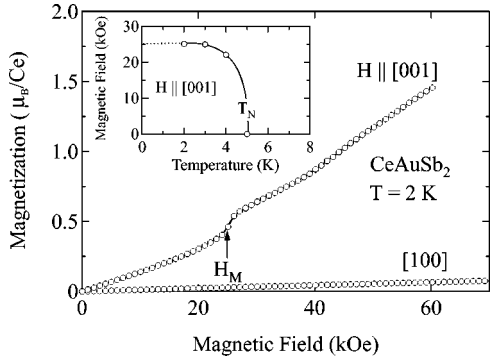

FIG. 8. Field dependence of the magnetization in $CeAuSb_2$. The magnetic phase diagram for $H\|$ [001] is shown in the inset.

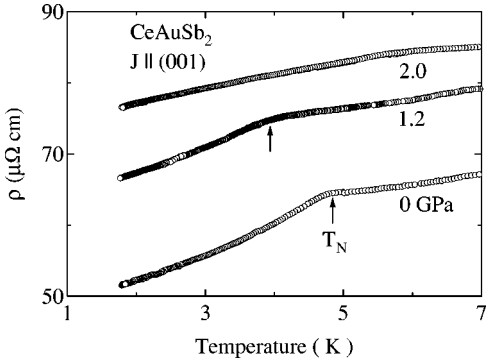

FIG. 10. Low-temperature resistivity of $CeAuSb_2$ for $J\|$ (001) under pressure. The arrow indicates the antiferromagnetic ordering.

In this compound, the susceptibility is also highly anisotropic. The susceptibility value for the field along [001] is much larger than that for [100], and for temperatures above 100 K, the susceptibility follows the Curie-Weiss law. The effective magnetic moment and the paramagnetic Curie temperature are $\mu_{\text{eff}}=2.50\mu_B$/Ce and $\theta_p=-69$ K, respectively, for $H\|$ [100], and $\mu_{\text{eff}}=2.49\mu_B$/Ce and $\theta_p=21$ K, respectively, for $H\|$ [001].

The antiferromagnetic ordering is further confirmed by the magnetization. The field dependence of magnetization at 2 K for two principal directions is shown in Fig. 8. For $H\|$ [100], the magnetization increases linearly up to 70 kOe, whereas the magnetization for $H\|$ [001] is linear up to 25 kOe but shows a metamagnetic transition at 25 kOe. The value of magnetization at 60 kOe is $1.5\mu_B$/Ce, while the value for $H\|$ [100] is $0.08\mu_B$/Ce, indicating highly anisotropic magnetizations. The metamagnetic transition disappears in the paramagnetic phase. The magnetic phase diagram is shown in the inset of Fig. 8.

The temperature dependence of the heat capacity in the form of C/T is shown in Fig. 9. A peak clearly indicates the bulk antiferromagnetic ordering in this compound. The temperature dependence of C/T below 3 K is almost linear, and the γ value is estimated by the linear extrapolation below 3 K to be about 90 mJ/K^2 mol, as shown by a broken line in Fig. 9. As can be seen from Fig. 9, the total entropy at the magnetic ordering temperature is about $0.5R\ln 2$, similar to the case of $CeCuSb_2$. The magnetic and thermal properties of $CeAuSb_2$ are summarized in Table I.

We have also studied the pressure dependence of the resistivity. Figure 10 shows the low-temperature part of the electrical resistivity for different applied pressures. The resistivity shifts in the vertical scale with increasing applied pressure. As can be seen from the figure, the Néel temperature T_N decreases with increasing pressure and becomes zero at about 2.0 GPa.

C. $CeNiSb_2$

The temperature dependence of the electrical resistivity of $CeNiSb_2$ is shown in Fig. 11. The resistivity behavior is quite different from that of $CeCuSb_2$ and $CeAuSb_2$. For $CeNiSb_2$ a broad hump is observed around 100 K. This could be caused by the interplay between the CEF and the Kondo effect.[17] For temperatures below 50 K, the resistivity shows a local minimum around 25 K and upon further cooling, the resistivity passes through a maximum at 7 K and then drops steeply due to the magnetic ordering below $T_C=6.0$ K. Previous report on the polycrystalline sample of $CeNiSb_2$ by Muro *et al.*[12] indicated no magnetic ordering. However, another study on the polycrystalline sample by Vijaya Lakshmi *et al.*[18] have indicated the magnetic ordering in this compound around 6 K, although their absolute value of resistivity is very high compared to our data. This could be due to the single-crystalline nature of our sample.

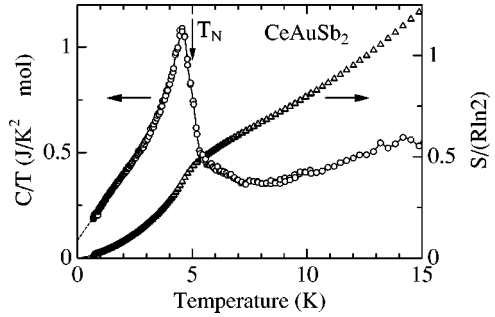

FIG. 9. Temperature dependence of the specific heat and the total entropy of $CeAuSb_2$. The broken line is a linear extrapolation of C/T data below 3 K, and the solid line shows the corresponding entropy change.

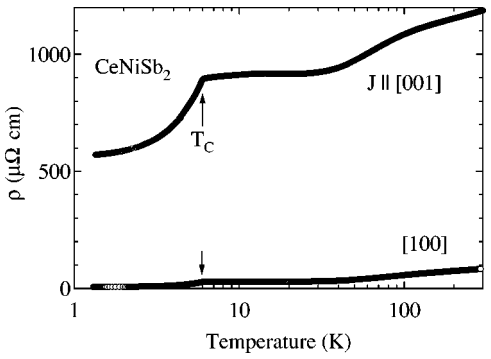

FIG. 11. Temperature dependence of the electrical resistivity in $CeNiSb_2$.

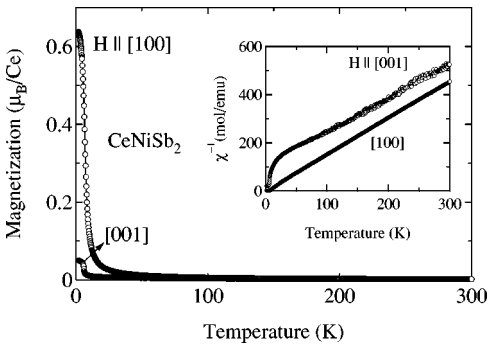

FIG. 12. Temperature dependence of magnetization. The inset shows the inverse magnetic susceptibility of $CeNiSb_2$.

The temperature dependence of magnetization in a field of 5 kOe is shown in Fig. 12. The ferromagnetic ordering in this compound is observed by the inflection point at 6.0 K in the magnetization versus temperature curve. The inverse susceptibility plot of $CeNiSb_2$ is shown in the inset of Fig. 12. The high-temperature data follow the Curie-Weiss law with the effective magnetic moment of $2.30\mu_B$/Ce and $2.38\mu_B$/Ce, respectively, for $H\|$ [100] and $H\|$ [001] and the estimated paramagnetic Curie temperature amounts to 0.3 K and -72 K, respectively, for $H\|$ [100] and $H\|$ [001].

The magnetization curve at 2 K in Fig. 13 shows a considerable deviation from linear behavior, and a hysteresis in the magnetization curve is observed along $H\|$ [100] and $H\|$ [110], consistent with the notion of the ferromagnetic ordering in this compound. The magnetization increases very rapidly for small applied fields along [100] and saturates around 25 kOe with a saturation moment of $0.6\mu_B$/Ce, indicating [100] as the easy axis of magnetization.

The temperature dependence of specific heat in the form of C/T and the total entropy is shown in Fig. 14. The data show a clear jump at $T_C = 6.0$ K, displaying the bulk ferromagnetic transition, which is in accordance with the resistivity and the susceptibility measurements. The C/T data below 2 K can be described by an equation of $C/T = \gamma + \beta T^2 + AT^{1/2}$, with parameters $\gamma = 55$ mJ/K^2 mol, $\beta = 56$ mJ/K^4 mol, and $A = 6$ mJ/K$^{5/2}$ mol, assuming spin-wave excitations in the ferromagnets, as shown by a broken line in Fig. 14. The total entropy at T_C is found to be $0.5R \ln 2$. The magnetic and thermal properties of $CeNiSb_2$ are summarized in Table I.

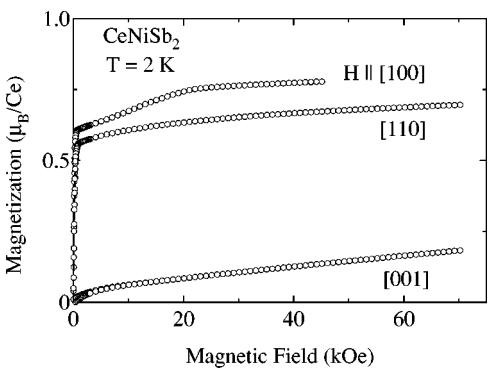

FIG. 13. Field dependence of magnetization in $CeNiSb_2$.

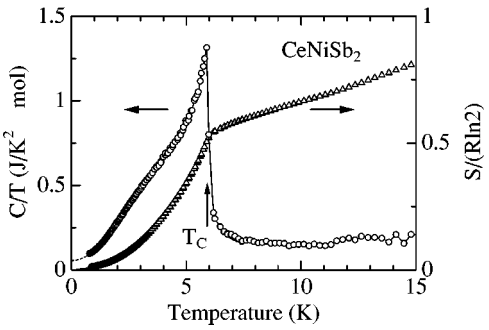

FIG. 14. Temperature dependence of the specific heat and the total entropy of $CeNiSb_2$. Broken and solid lines are the fitting curve and the corresponding entropy change, respectively.

IV. DISCUSSION

As shown in the preceding section, the magnetic properties of CeTSb$_2$ are largely dependent on the kind of transition metal T. $CeCuSb_2$ and $CeAuSb_2$ show antiferromagnetic order at low temperatures, while $CeNiSb_2$ has a ferromagnetic ground state below 6.0 K. The variations of the magnetic anisotropy are more intriguing. In $CeCuSb_2$, the magnetic anisotropy is very small as shown in Fig. 3, although the resistivity shows an anisotropic feature, as shown in Fig. 2, suggesting a quasi-two-dimensional electronic state. On the other hand, $CeAuSb_2$ and $CeNiSb_2$ show a large magnetic anisotropy, although the magnetic easy axis is interchanged with respect to each other, namely, [001] for the antiferromagnet $CeAuSb_2$ and [100] for the ferromagnet $CeNiSb_2$. These facts imply that the CEF as well as the Ruderman-Kittel-Kasuya-Yosida interaction in CeTSb$_2$ are significantly influenced by the transition metal. The total entropy change for these compounds studied here amount to about $0.5R \ln 2$ at the ordering temperature. This suggests that the magnetism in all the three compounds is due to itinerant $4f$ electrons. However, the relatively large induced magnetic moments of $1.5\mu_B$/Ce and $0.8\mu_B$/Ce at 60 kOe for $CeAuSb_2$ and $CeNiSb_2$, respectively, indicate that the moment reduction due to the Kondo effect is small for at least these two compounds. Therefore, we concluded that the $4f$ electrons are nearly localized in these compounds, and analyzed the magnetic susceptibility and magnetization data on the basis of a simple CEF model to see the CEF effect on the anisotropy change. The CEF Hamiltonian for tetragonal symmetry is given by

$$\mathcal{H}_{\mathrm{CEF}} = B_2^0 O_2^0 + B_4^0 O_4^0 + B_4^4 O_4^4, \tag{1}$$

where B_ℓ^m and O_ℓ^m are the CEF parameters and the Stevens operators, respectively.[19,20] The CEF susceptibility is defined as

$$\chi_{\mathrm{CEF}i} = N(g_J\mu_B)^2 \frac{1}{Z}\left(\sum_{m\neq n} |\langle m|J_i|n\rangle|^2 \frac{1-e^{-\beta\Delta_{m,n}}}{\Delta_{m,n}} e^{-\beta E_n} + \sum_n |\langle n|J_i|n\rangle|^2 \beta e^{-\beta E_n} \right), \tag{2}$$

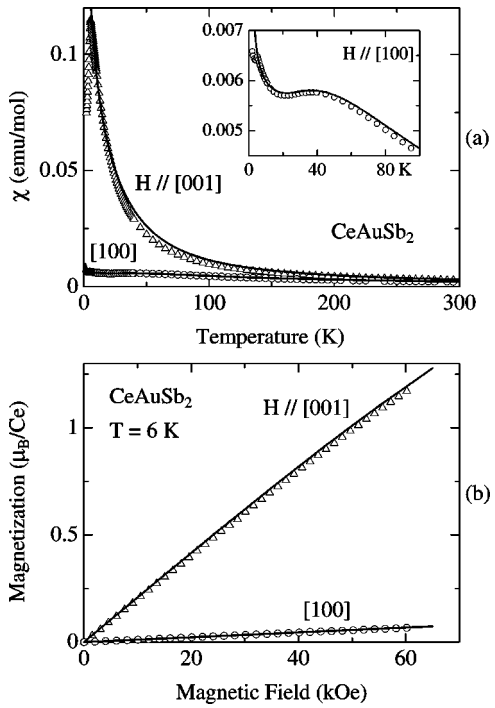

FIG. 15. (a) Magnetic susceptibility and (b) magnetization curves of $CeAuSb_2$. The solid lines are the calculated curves as described in the text and the inset in (a) shows the low-temperature part of the susceptibility for $H \| [100]$.

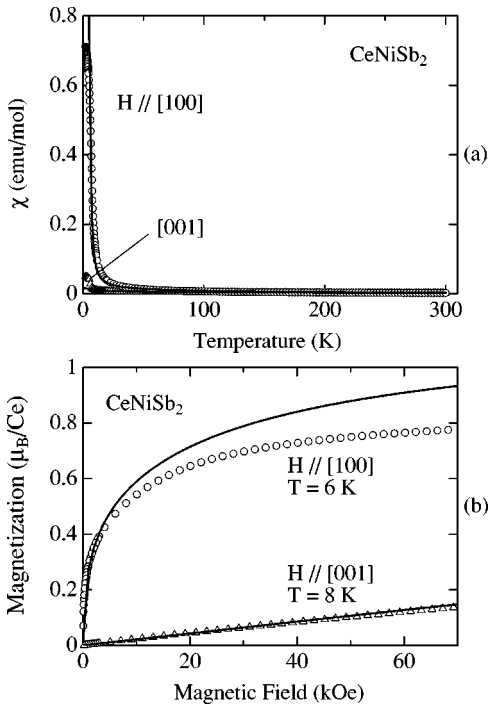

FIG. 16. (a) Magnetic susceptibility and (b) magnetization curves of $CeNiSb_2$. The solid lines are the calculated curves as explained in the text.

where g_J is the Landé g factor ($=6/7$ for Ce^{3+}), E_n and $|n\rangle$ are the nth eigenvalue and eigenfunction, respectively. J_i ($i=x,y$, and z) is the component of the angular momentum, $\Delta_{m,n}=E_n-E_m$, $Z=\Sigma_n e^{-\beta E_n}$, and $\beta=1/k_BT$. The magnetic susceptibility including the molecular-field contribution λ_i is given by

$$\chi_i^{-1}=\chi_{\mathrm{CEF}i}^{-1}-\lambda_i. \tag{3}$$

We have also calculated the magnetization by using the following formula:

$$M_i=g_J\mu_B\sum_n |\langle n|J_i|n\rangle|\frac{e^{-\beta E_n}}{Z}, \tag{4}$$

where the eigenvalue E_n and the eigenfunction $|n\rangle$ are determined by diagonalizing the total Hamiltonian

$$\mathcal{H}=\mathcal{H}_{\mathrm{CEF}}-g_J\mu_B J_i(H+\lambda_i M_i), \tag{5}$$

where $\mathcal{H}_{\mathrm{CEF}}$ is given by Eq. (1), the second term is the Zeeman term, and the third one is the molecular field.

The CEF parameters were estimated from the fits to the magnetic susceptibility and magnetization data. Solid lines in Figs. 15 and 16 show the calculated curves by using the CEF

TABLE II. CEF parameters, energy-level schemes, and the corresponding wave functions for $CeAuSb_2$.

CEF parameters						
	B_2^0 (K)	B_4^0 (K)	B_4^4 (K)	λ_i (emu/mol)$^{-1}$		
	-8	0	0.3	$\lambda_{[100]}=-40$		
				$\lambda_{[001]}=-5$		
Energy levels and wave functions						
E(K)	$\|+5/2\rangle$	$\|+3/2\rangle$	$\|+1/2\rangle$	$\|-1/2\rangle$	$\|-3/2\rangle$	$\|-5/2\rangle$
145	0	0	1	0	0	0
145	0	0	0	1	0	0
97	0	-0.997	0	0	0	-0.083
97	0.083	0	0	0	0.997	0
0	0	-0.083	0	0	0	-0.997
0	-0.997	0	0	0	0.083	0

TABLE III. CEF parameters, energy-level schemes, and the corresponding wave functions for $CeNiSb_2$.

CEF parameters						
	B_2^0 (K)	B_4^0 (K)	B_4^4 (K)	λ_i (emu/mol)$^{-1}$		
	7	0.3	6	$\lambda_{[100]}=19$		
				$\lambda_{[001]}=19$		
Energy levels and wave functions						
E(K)	$\|+5/2\rangle$	$\|+3/2\rangle$	$\|+1/2\rangle$	$\|-1/2\rangle$	$\|-3/2\rangle$	$\|-5/2\rangle$
358	0	−0.531	1	0	0	−0.847
358	0.847	0	0	0	0.531	0
149	0	0	1	0	0	0
149	0	0	0	1	0	0
0	0	0.847	0	0	0	−0.531
0	0.531	0	0	0	−0.847	0

parameters listed in Tables II and III for $CeAuSb_2$ and $CeNiSb_2$, respectively.

As shown in Figs. 15(a) and 15(b), we get good fits with the proposed CEF model for susceptibility and magnetization of $CeAuSb_2$. On the other hand, there is a difference between the experimental and calculated magnetization curves for $H\|[100]$ in $CeNiSb_2$, as shown in Fig. 16(b). With regards to $CeCuSb_2$, the small magnetic anisotropy leads to a very small energy splitting with less than 10 K of the CEF scheme. Small induced magnetizations at 70 kOe (about $0.45\mu_B$/Ce) and the relatively large γ value (100 mJ/K^2 mol) may imply a substantial Kondo effect which should be considered in the analysis of the magnetic properties of $CeCuSb_2$.

Very recently, we have reported that the magnetic properties in $CeAgSb_2$ can be well understood by the CEF model.[15] In this CEF scheme, the wave functions of the ground state are $|\pm 1/2\rangle$ and the observed ferromagnetic moment of about $0.4\mu_B$/Ce along [001] is explained by the saturation moment of the ground state, $g_J\mu_B J_z = 0.43\mu_B$/Ce. Considering this fact, we suggest the hybridization strength decreases from $CeCuSb_2$ to $CeAuSb_2$. It is noted that a similar tendency was reported for CeT_2Si_2 ($T=$ transition metal) system, where well-defined CEF excitations were observed in $CeAg_2Si_2$ and $CeAu_2Si_2$, while only a broadened excitation, which is due to the strong interactions between f electrons and conduction bands, was detected for $CeCu_2Si_2$.[21]

The present anisotropy change between $CeAuSb_2$ and $CeNiSb_2$ is reflected to the sign of the B_2^0 parameter as shown in Tables II and III: $B_2^0 = -8$ K in $CeAuSb_2$ and $B_2^0 = 7$ K in $CeNiSb_2$. Even in $CeAgSb_2$ whose transition-metal element is located just one above Au in the periodic table, the sign of the B_2^0 ($=7.8$ K) is opposite to that in $CeAuSb_2$.[15] When Coulomb interactions with neighboring ions have a dominant effect to the CEF potential, it seems that the sign of B_2^0 should be the same even if we change the transition-metal element. The dramatic change of the sign in the B_2^0 parameter suggests that the CEF potential in $CeTSb_2$ is largely dependent on the hybridization between localized f-electron states and the conduction-electron bands.[22] In addition to the c-f mixing effect, which is responsible for the development of the heavy-fermion state, a mixing effect between f electrons in Ce and p electrons in Sb may be another possibility for the presence of such hybridization effects, because $CeTSb_2$ consists of a sequential stacking of CeSb-T-CeSb-Sb layers along the [001] direction. In fact, a quasi-two-dimensional electronic state was observed in $CeAgSb_2$ by the dHvA experiment.[14] A detailed systematic neutron-scattering and high-temperature specific-heat measurements are necessary to substantiate our calculations about the level splitting and to clarify the influence of the hybridization effect on the CEF state in $CeTSb_2$.

V. SUMMARY

We have investigated the electrical and magnetic properties of $CeCuSb_2$, $CeAuSb_2$, and $CeNiSb_2$. The electrical resistivity is highly anisotropic between $J\|$ [100] and [001], indicating a quasi-two-dimensional electronic state. $CeCuSb_2$ and $CeAuSb_2$ are antiferromagnets with $T_N = 6.9$ K and 5.0 K, respectively. The antiferromagnetic easy axis in $CeAuSb_2$ is along [001]. The Néel temperature decreases with increasing pressure for $CeAuSb_2$. $CeNiSb_2$ is a ferromagnet with $T_C = 6.0$ K. The easy axis in $CeNiSb_2$ is along [100]. The relatively large γ values in these compounds, in the magnetically ordered state, suggest the strong electron correlations.

ACKNOWLEDGMENTS

We would like to thank Professor S. Ramakrishnan for a critical reading of this manuscript. The present work was financially supported by a Grant-in-Aid for Scientific Research COE (Grant No. 10CE2004) from the Ministry of Education, Culture, Sports, Science and Technology. One of the authors (A.T.) is very much grateful to the Japanese Society for Promotion of Science (JSPS) for financial assistance.

[1] J.D. Thompson, R. Movshovich, Z. Fisk, F. Bouquet, N.J. Curro, R.A. Fisher, P.C. Hammel, H. Hegger, M.F. Hundley, M. Jaime, P.G. Pagliuso, C. Petrovic, N.E. Phillips, and J.L. Sarrao, J. Magn. Magn. Mater. **226-230**, 5 (2001).

[2] C. Petrovic, P.G. Pagliuso, M.F. Hundley, R. Movshovich, J.L. Sarrao, J.D. Thompson, Z. Fisk, and P. Monthoux, J. Phys.: Condens. Matter **13**, L337 (2001).

[3] H. Shishido, R. Settai, D. Aoki, S. Ikeda, H. Nakawaki, N. Nakamura, T. Iizuka, Y. Inada, K. Sugiyama, T. Takeuchi, K. Kindo, T.C. Kobayashi, Y. Haga, H. Harima, Y. Aoki, T. Namiki, H. Sato, and Y. Onuki, J. Phys. Soc. Jpn. **71**, 162 (2002).

[4] K. Izawa, H. Yamaguchi, Y. Matsuda, H. Shishido, R. Settai, and Y. Onuki, Phys. Rev. Lett. **87**, 057002 (2001).

[5] S.L. Bud'ko, P.C. Canfield, C.H. Mielke, and A.H. Lacerda, Phys. Rev. B **57**, 13 624 (1998).

[6] Y. Onuki, D. Aoki, P. Wisniewski, H. Shishido, S. Ikeda, Y. Inada, Y. Koike, E. Yamamoto, Y. Haga, T. Maehira, H. Harima, M. Higuchi, A. Hasegawa, and H. Yamagami, Acta Phys. Pol. B **32**, 3273 (2001).

[7] R. Settai, Y. Yoshida, A. Yamaguchi, Y. Onuki, S. Yoshii, M. Kasaya, H. Harima, and K. Takegahara, J. Phys. Soc. Jpn. **68**, 3615 (1999).

[8] D. Kaczorowski, R. Kruk, J.P. Sanchez, B. Malaman, and F. Wastin, Phys. Rev. B **58**, 9227 (1998).

[9] M. Brylak, M.H. Möller, and W. Jeitschko, J. Solid State Chem. **115**, 305 (1995).

[10] H. Flandorfer, O. Sologub, C. Godart, K. Hiebl, A. Leithe-Jasper, P. Rogl, and H. Noël, Solid State Commun. **97**, 561 (1996).

[11] M. Houshiar, D.T. Adroja, and B.D. Rainford, J. Magn. Magn. Mater. **140-144**, 1231 (1995).

[12] Y. Muro, N. Takeda, and M. Ishikawa, J. Alloys Compd. **257**, 23 (1997).

[13] K.D. Myers, S.L. Bud'ko, I.R. Fisher, Z. Islam, H. Kleinke, A.H. Lacerda, and P.C. Canfield, J. Magn. Magn. Mater. **205**, 27 (1999).

[14] Y. Inada, A. Thamizhavel, H. Yamagami, T. Takeuchi, Y. Sawai, S. Ikeda, H. Shishido, T. Okubo, M. Yamada, K. Sugiyama, N. Nakamura, T. Yamamoto, K. Kindo, T. Ebihara, A. Galatanu, E. Yamamoto, R. Settai, and Y. Onuki, Philos. Mag. B **82**, 1867 (2002).

[15] T. Takeuchi, A. Thamizhavel, T. Okubo, M. Yamada, N. Nakamura, T. Yamamoto, Y. Inada, K. Sugiyama, A. Galatanu, E. Yamamoto, K. Kindo, T. Ebihara, and Y. Onuki, Phys. Rev. B **67**, 064403 (2003).

[16] Y. Onuki and T. Komatsubara, J. Magn. Magn. Mater. **63&64**, 281 (1987).

[17] B. Cornut and B. Coqblin, Phys. Rev. B **5**, 4541 (1972).

[18] K. Vijaya Lakshmi, Latika Menon, A.K. Nigam, A. Das, and S.K. Malik, Physica B **223&224**, 289 (1996).

[19] K.W.H. Stevens, Proc. Phys. Soc., London, Sect. A **65**, 209 (1952).

[20] M.T. Hutchings, in *Solid State Physics: Advances in Research and Applications*, edited by F. Seitz and B. Turnbull (Academic, New York, 1965), Vol. 16, p. 227.

[21] A. Severing, E. Holland-Moritz, B.D. Rainford, S.R. Culverhouse, and B. Frick, Phys. Rev. B **39**, 2557 (1989).

[22] P.M. Levy and S. Zhang, Phys. Rev. Lett. **62**, 78 (1989).